An Improved Relative Permeability Model to Match Displacement Experiments

Mohammed Idrees Al-Mossawy (Corresponding Author)
Geoscience & Petroleum Engineering Department
Universiti Teknologi PETRONAS
(Petronas University of Technology)
Bandar Seri Iskandar, 31750 Tronoh, Perak Darul Ridzuan
Malaysia
E-mail: mohm63@yahoo.com

Birol Demiral
Petroleum Engineering & Geoscience Department
Universiti Teknologi PETRONAS
(Petronas University of Technology)
Bandar Seri Iskandar, 31750 Tronoh, Perak Darul Ridzuan
Malaysia
E-mail: birol_demiral@petronas.com.my

Abstract

In petroleum industry due to existence of gas and liquid phases in hydrocarbon reservoirs, the relative permeability data are essential to the reservoir simulation. The relative permeability test can be conducted either by the steady-state flow method or the unsteady-state flow method. The present model is derived for the unsteady-state displacement method. It considers effects of fluids viscosities and the average saturation at the breakthrough moment in addition to the parameters considered by previous models. First a preliminary model was derived from a function of porosity and permeability called poroperm. Then the fractional flow theory was used to improve the preliminary model to match the actual displacement process. The improved model was implemented on experimental data of seven Berea sandstone cores. Comparison of results with three models showed that the present model is the perfect.

Key Words: Relative permeability; Poroperm; Fluid flow in porous media

1 Introduction

Multiphase flow in porous media is a complex problem. Relative permeability is the practical way to describe flow of one phase in presence of other phases. In petroleum industry due to the fact that nearly all hydrocarbon reservoirs contain more than one flowing phase, the relative permeability data are essential for simulation studies of oil reservoirs. Relative permeability data should be obtained by experiments that best model the type of displacement that is thought to dominate reservoir flow performance (Fanchi 2001). The relative permeability test can be conducted either by the steady-state flow method or unsteady-state flow method **(**Ibrahim and Koederitz 2001; Torsæter and Abtahi 2003; Tiab and Dnaldson 2004). The steady-state method has an advantage of simple calculations, and disadvantage of tedious long procedure.

The unsteady-state method takes less time but requires more complicated calculations (Jones and Roszelle 1978; Mitlin et al. 1998; Toth et al. 1998; Bech et al. 2000; Toth et al. 2001). To improve or simplify calculations of the unsteady-state method, different models have been published based on the initial and final stages of the flow process (Corey 1954; Wyllie and Gardner 1958; Torcaso and Wyllie 1958; Pirson 1958; Honarpour et al. 1982; Ahmed 2001a; Ibrahim and Koederitz 2000; Behrenbruch and Goda 2006). Other techniques have been used to predict the relative permeability such as artificial neural networks (Silpngarmlers et al. 2002), and resistivity data (Li 2008; Li et al. 2010). Bang et al. (2006) presented correlation for relative permeability of gas-condensate fluids. Details of laboratory measurements and correlations for the relative permeability were presented by Honarpour et al. (1986). The most utilized model by the petroleum industry is the modified Brooks and Corey (MBC) model (Alpak et al. 1999; Behrenbruch and Goda 2006):

$$K_{r1} = K_{r1}^{*}\left(\frac{S_1 - S_{1r}}{1 - S_{1r} - S_{2r}}\right)^{n_1} \qquad (1)$$

$$K_{r2} = K_{r2}^{*}\left(\frac{1-S_1-S_{2r}}{1-S_{1r}-S_{2r}}\right)^{n_2} \quad (2)$$

where K^*_{r1} and K^*_{r2} are end-point relative permeabilities for phases 1 and 2, S_{1r} and S_{2r} are residual saturations for phases 1 and 2, and n_1 and n_2 are exponents to be fit to the experimental data. Behrenbruch and Goda (2006) showed that values of n_1 and n_2 are a measure of the degree of heterogeneity of the core plugs, rather than wettability. MBC model cannot predict a relative permeability relationship, rather it is intended to smooth and extend an existing relationship (Behrenbruch and Goda 2006).

The present study aims to derive an improved relative permeability model can matching the displacement process. The model starts from deriving a function of porosity and permeability called poroperm to represent the dynamic pore connectivity of porous media. This function is assumed having a specific constant value for each fluid during the displacement process. This leads to a preliminary model to determine the relative permeability. To represent the actual displacement process considering heterogeneity and wettability of the porous medium, and fluids rheology, the exponent of the preliminary model is replaced by one calculated from Welge's method (1952) of fractional flow theory. The improved model has been implemented on experimental data. Seven core plugs of Berea sandstone with different porosity and permeability have been used in the experiments. Nitrogen gas was used to displace brine from the cores. Results of the present model were compared with three published models. The present model was the perfect for the seven cases.

2 Poroperm Function

It is suggested that any porous medium with known porosity and permeability can be represented by a virtual capillary-bundle has number (n) of straight capillaries with an average diameter (d_c). Equations can be derived to find n and d_c from solving simultaneously Darcy's law, Poiseuille's law, and definition of porosity. Both n and d_c reflect relationships between the porosity and permeability and can be used to characterize the pore connectivity in the direction at which the permeability had been measured.

For the cylindrical core sample the flow rate (Q cm^3/sec) along its axis from Darcy's law is:

$$Q = \frac{(1.01325\,\mathrm{K})\left(\frac{\pi D^2}{4}\right)\left(\frac{\Delta P}{1.01325}\right)}{\mu L} \quad (3)$$

where K is the absolute permeability (μm^2), D is the core diameter (cm), ΔP is the pressure drop (bar), μ is viscosity of the flowing fluid (mPa.sec), and L is the core length (cm). The same flow rate through a capillary-bundle can be represented by the general form of Poiseuille's law:

$$Q = \sum_{i=1}^{i=n} q_i = \frac{n\left(\frac{d_c}{2}\right)^4 \pi \Delta P\, C_1}{8\mu L} \quad (4)$$

where C_1 is a factor to convert units to be consistent with Darcy's law units, n is number of capillaries, and d_c is the average diameter of capillaries (cm). Substituting Q from Eq. (3) in Eq. (4) gives following Eq.:

$$K = \frac{n\, d_c^{\,4}}{C_2\, D^2} \quad (5)$$

where C_2 is a units conversion factor . Eq. (5) is equivalent to Eq. (7.30) of (Tiab and Dnaldson 2004). Porosity of the core can be defined as follows:

$$\phi = \frac{Pore Volume}{Bulk Volume} = \frac{n\left(\frac{\pi d_c^{\,2}}{4}\right)L}{\left(\frac{\pi D^2}{4}\right)L} = \frac{n d_c^2}{D^2} \quad (6)$$

Solving Eqs. (5) and (6) simultaneously for n and d_c gives:

$$n = \frac{C_3\left(\phi D\right)^2}{K} \quad (7)$$

and

$$d_c = C_4 \sqrt{\frac{K}{\phi}} \quad (8)$$

where $C_3 = 3.125\times10^6$ and $C_4 = 5.656\times10^{-4}$. For porous media with high dynamic pore connectivity, n will be low and d_c will be high, and vice versa. For porous media having different shapes, D can be obtained from the following Eq.:

$$D = \sqrt{\frac{4A}{\pi}} \quad (9)$$

where A = cross-sectional area perpendicular to the flow direction.

To convert the number of capillaries function (n) to a generalized function independent of the core diameter and has practical units, poroperm function (P_p) is defined as the inverse of n for flow through a cross-sectional area of 1μm^2. Mathematically it can be obtained by substituting A = 1μm^2 into Eq. (9) then determining the inverse of n from Eq. (7). Thus:

$$P_p = \frac{25.133\,K}{\phi^2} \quad (10)$$

where P_p and K have the same units. Fig. 1 shows the relationship between the poroperm function and the porosity at different permeabilities.

3 Preliminary Model of Relative Permeability

Dynamic pore connectivity of porous media during the two-phase flow can be derived from end points of the relative permeability curves. The poroperm function of each phase can be calculated from the effective permeability and effective porosity at the end points. Assuming that poroperm function of each phase remains constant, and the effective permeability is just a function of the saturation, leads to capability of calculating the effective and relative permeability at any saturation. This concept is clarified in Fig. 2, and it agrees with base of MBC model (Eqs. 1 and 2). Thus the relative permeability from poroperm can be derived as follows:
For two-phase flow in a porous medium, P_p of any phase of them can be obtained by substituting the effective porosity and permeability in Eq. 10:

$$P_p = \frac{25.133\,K_{eff\,1}}{\phi_{eff\,1}^{\,2}} = \frac{25.133\,K_{eff\,2}}{\phi_{eff\,2}^{\,2}} \quad (11)$$

where K_{eff1} and K_{eff2} are the effective permeabilities at the effective porosities φ_{eff1} and φ_{eff2} for the same phase, respectively. The effective porosity is defined as:

$$\phi_{eff} = \phi S \quad (12)$$

where φ is the total porosity, and S is the phase saturation. Substituting Eq. 12 in Eq. 11 yields:

$$K_{eff\,2} = K_{eff\,1}\left(\frac{S_2}{S_1}\right)^2 \quad (13)$$

Dividing both sides of Eq. 13 by the absolute permeability yields:

$$K_{r2} = K_{r1}\left(\frac{S_2}{S_1}\right)^2 \quad (14)$$

where K_{r1} and K_{r2} are relative permeabilities of the same phase at saturations S_1 and S_2, respectively. Eq. 14 can be used to generate relative permeability curves from measuring relative permeabilities of fluids at end points of the displacement process. To verify the model, it will be implemented on a process of displacing water from a core plug by injecting gas. Figs. 3 shows typical relative permeability curves of the drainage and imbibition cycles of water-gas flow process in a core was initially saturated with water. Implementing Eq. 14 to the relative permeability curves of Fig. 3 yields:

$$K_{rg} = K_{rgwc}\left(\frac{1-S_w-S_{gc}}{1-S_{wc}-S_{gc}}\right)^2 \quad (15)$$

and

$$K_{rw} = K_{rwgc}\left(\frac{S_w - S_{wc}}{1 - S_{wc} - S_{gc}}\right)^2 \qquad (16)$$

where K_{rgwc} is gas relative permeability at the irreducible water saturation (S_{wc}), K_{rwgc} is water relative permeability at the critical (or residual) gas saturation (S_{gc}), and K_{rg} and K_{rw} are relative permeabilities of gas and water at any water saturation (S_w), respectively. Eqs. 15 and 16 have the same forms of Eqs. 1 and 2 of MBC model with specifying exponents values by 2. This approves that the assumption of remaining of the dynamic pore connectivity (was represented by the poroperm function) constant for each phase, is involved implicitly in MBC model (Eqs. 1 and 2).

4 Improved Model of Relative Permeability

To adjust the preliminary model to consider heterogeneity and wettability of porous media, and fluid rheology, Eqs. 15 and 16 can be modified to be:

$$K_{rg} = K_{rgwc}\left(\frac{1 - S_w - S_{gc}}{1 - S_{wc} - S_{gc}}\right)^a \qquad (17)$$

and

$$K_{rw} = K_{rwgc}\left(\frac{S_w - S_{wc}}{1 - S_{wc} - S_{gc}}\right)^a \qquad (18)$$

where *a* is an empirical exponent to formulate a model satisfies all conditions of the displacement process. To determine value of the exponent (a) it is required determining the average water saturation in the core at the breakthrough moment experimentally, then using the fractional flow theory. The procedure includes the following steps:

1. To recode water flow rate at the outlet of the core plug as a function of time.
2. To calculate the average water saturation from the material balance equation as a function of time.
3. To plot water flow rate versus the average water saturation (see Fig. 4), and determine the average water saturation behind the front at moment of gas breakthrough ($(S_{wavg})_{Bth}$).
4. To use the fractional flow theory. Neglecting the effects of gravity and capillary pressure gradient, the fractional flow equation can be written as follows (Dake 1978; Ahmed 2001b):

$$f_w = \frac{1}{1 + \frac{K_{rg}}{K_{rw}}\frac{\mu_w}{\mu_g}} \qquad (19)$$

where f_w is the water fractional flow, μ_w and μ_g are water and gas viscosities (mPa.sec), respectively. The gas/water relative-permeability ratio is obtained from dividing Eq. 17 by Eq. 18:

$$\frac{K_{rg}}{K_{rw}} = \left(\frac{K_{rgwc}}{K_{rwgc}}\right)\left(\frac{1 - S_w - S_{gc}}{S_w - S_{wc}}\right)^a \qquad (20)$$

Substituting Eq. 20 in Eq. 19 yields:

$$f_w = \frac{1}{1 + \frac{\mu_w}{\mu_g}\left(\frac{K_{rgwc}}{K_{rwgc}}\right)\left(\frac{1 - S_w - S_{gc}}{S_w - S_{wc}}\right)^a} \qquad (21)$$

Welge (1952) showed that $(S_{wavg})_{Bth}$ can be determined graphically by drawing a tangent to the curve of $f_w(S_w)$, starting from the initial point (S_w =1- S_{gc}) to intercept the line f_w = zero at the point (S_w = $(S_{wavg})_{Bth}$, f_w = zero) (see Fig. 5). Equation of the tangent is:

$$f_w = \frac{S_w - (S_{wavg})_{Bth}}{1 - S_{gc} - (S_{wavg})_{Bth}} \qquad (22)$$

Water saturation and water fractional flow at the displacement front (S_{wf}) and (f_{wf}), respectively, satisfy simultaneously Eqs. 21 and 22 at the moment of gas breakthrough. When the displacing process is conducted by injecting a fixed flow rate of incompressible fluid, fractional flow of the injected fluid at the breakthrough moment can be determined experimentally, and the corresponding saturation can be calculated from equation of the tangent (Eq. 22). In this case the exponent (a) can be calculated directly from equation of the fractional flow (Eq. 21). In case of the displacing fluid is gas (as in our experiments) it could not be or difficult to determine the water fractional flow at the breakthrough moment experimentally because of gas compressibility. The exponent (a) can be determined by the following method. At the tangency point with co-ordinates ($S_w = S_{wf}$, $f_w = f_{wf}$), the derivative of fractional flow equation (Eq. 21) should be equal to the derivative of tangent equation (Eq. 22). Derivative of Eq. 21 at ($S_w = S_{wf}$) is:

$$\left(\frac{df_w}{dS_w}\right)_{S_{wf}} = \frac{\dfrac{a(1-S_{wc}-S_{gc})\mu_w K_{rgwc}}{(S_{wf}-S_{wc})(1-S_{wf}-S_{gc})\mu_g K_{rwgc}}\left(\dfrac{1-S_{wf}-S_{gc}}{S_{wf}-S_{wc}}\right)^a}{\left[1+\dfrac{\mu_w K_{rgwc}}{\mu_g K_{rwgc}}\left(\dfrac{1-S_{wf}-S_{gc}}{S_{wf}-S_{wc}}\right)^a\right]^2} \qquad (23)$$

From Eq. 21:

$$\frac{\mu_w K_{rgwc}}{\mu_g K_{rwgc}}\left(\frac{1-S_w-S_{gc}}{S_w-S_{wc}}\right)^a = \frac{1}{f_w}-1 \qquad (24)$$

Substituting Eqs. 21 and 24 for point (S_{wf}, f_{wf}) in Eq. 23 yields:

$$\left(\frac{df_w}{dS_w}\right)_{S_{wf}} = \frac{a(1-S_{wc}-S_{gc})\,f_{wf}^2}{(S_{wf}-S_{wc})(1-S_{wf}-S_{gc})}\left(\frac{1}{f_{wf}}-1\right) \qquad (25)$$

Derivative of Eq.22 at ($S_w = S_{wf}$) is:

$$\left(\frac{df_w}{dS_w}\right)_{S_{wf}} = \frac{1}{1-S_{gc}-(S_{wavg})_{Bth}} \qquad (26)$$

Equating Eq. 25 to Eq. 26 gives:

$$a = \frac{(S_{wf}-S_{wc})(1-S_{wf}-S_{gc})}{f_{wf}^2\left(\dfrac{1}{f_{wf}}-1\right)(1-S_{wc}-S_{gc})\left(1-S_{gc}-(S_{wavg})_{Bth}\right)} \qquad (27)$$

Substituting Eq. 22 at the point (S_{wf}, f_{wf}) in Eq. 27, and simplifying give:

$$a = \frac{(S_{wf}-S_{wc})\left(1-S_{gc}-(S_{wavg})_{Bth}\right)}{(1-S_{wc}-S_{gc})\left(S_{wf}-(S_{wavg})_{Bth}\right)} \qquad (28)$$

To find solution of Eq. 28, it requires another equation represents exponent (a) as a function of (S_{wf}). Equating Eq. 21 to Eq. 22 at point (S_{wf}, f_{wf}), and rearranging give:

$$a = \frac{\ln\left[\left(\dfrac{1-S_{wf}-S_{gc}}{S_{wf}-(S_{wavg})_{Bth}}\right)\left(\dfrac{\mu_g K_{rwgc}}{\mu_w K_{rgwc}}\right)\right]}{\ln\left(\dfrac{1-S_{wf}-S_{gc}}{S_{wf}-S_{wc}}\right)} \qquad (29)$$

Attempting to obtain an analytical solution from solving Eqs. 28, and 29 simultaneously was fruitless. A graphical method can be used. Plotting Eqs. 28 and 29 for the range ($(S_{wavg})_{Bth} < S_w < 1\text{-}S_{gc}$) on the same graph gives an intersection point represents the actual S_{wf} and exponent (a). Implementation of the method on experimental data is shown in section 5. We observed that always the intersection point is at the maximum value of the exponent (a) calculated from Eq. 29. So that Eq. 29 can be sufficient to obtain the exponent (a) and the actual S_{wf}. As it is shown in Eq. 29, the improvement that has been achieved by this model is to consider effects of fluids viscosities, saturation at the displacement front, and the average saturation behind the displacement front, in addition to saturations and relative permeabilities of the end points.

5 Displacement Experiments

Seven Berea sandstone cores were used in core-flooding experiments. Porosity of the cores was measured using Permeameter-Porosity Meter with nitrogen gas. The equipment designed to measure the porosity by method called "Boyle's law Single Cell Method for direct void volume measurement". Then the cores were saturated with brine of (2.4 wt% of NaCl) in a special saturation cell. Table 1 shows density and viscosity of the brine and nitrogen gas at room conditions. The saturation process included evacuating cores from air till reaching the minimum pressure (-1 barg), then injecting brine into the saturation cell containing the cores. The cores were kept in the brine under pressure of (124 barg) for (16 hours). Measurement of permeability to brine, and displacing brine by nitrogen gas were conducted by a Bench Top Permeability System. Fig. 6 shows diagram of this system. The confining pressure was 28 barg, and the outlet pressure was the atmospheric pressure. Three different flow rates of brine were used for each core to measure the average absolute permeability. The brine was displaced from cores by injecting a fixed flow rate of (22.66 cm^3/min) of nitrogen gas at room conditions. Mass of water recovery was measured by a digital balance and then the volume was calculated from the mass and density.

Differential pressure and water recovery were recorded as functions of time. Average water saturation in the core as a function of time, was calculated from the material balance equation. $(S_{wavg})_{Bth}$ was determined from plotting the water flow rate at the core outlet as a function of the average water saturation (S_{wavg}). Initially the water flow rate increases since the water saturation at the outlet is still at its initial value ($S_w = 1$), and the water flow rate will be stable if there is no more effect of gas compressibility. Then the water flow rate will start decreasing at the gas breakthrough moment as a result of decreasing of the water saturation at the core outlet. Figs. 4 and 7 show determination of $(S_{wavg})_{Bth}$ from the experimental data for cores A and C, respectively. Fig. 4 shows decrease of water flow rate at the gas breakthrough moment before it reaching to a stable state. Fig. 7 shows a stable water flow rate before the gas breakthrough point. Some times the water flow rate at the outlet of the core experiences oscillations because of the gas compressibility or slipping of some of separate bubbles of gas ahead of the actual breakthrough of the continuous gas stream. Careful is required to determine $(S_{wavg})_{Bth}$ in such cases. Fig. 8 shows example of oscillation of the water flow rate before the gas breakthrough.

For the drainage process in a core initially was saturated with water, Fig. 3 shows that it can be practically considered the critical gas saturation (S_{gc}) has value of (zero) and water relative permeability at that saturation (K_{rwgc}) has value of (1). The relative permeability of gas at the irreducible water saturation (K_{rgwc}) was calculated as the ratio of gas effective permeability to the absolute permeability. The gas effective permeability was calculated from Darcy's law of gases. Table 2 shows properties of cores and results of gas relative permeability at the irreducible water saturation. To determine the exponent (a), Eqs. 28 and 29 was plotted for the range of ($(S_{wavg})_{Bth} < S_w < 1\text{-}S_{gc}$) on the same graph. The intersection point represents the actual S_{wf}, and exponent (a). Fig. 9 shows determination of the actual S_{wf}, and exponent (a) of core A. The water fractional flow at the front (f_{wf}) can be calculated either from Eq. 21 or Eq. 22. Table 3 shows results of the average water saturation at the breakthrough moment, exponent (a), and water saturation and fractional flow at the front. It is observed that the exponent (a) was in the range between (1.5) to (3). Since the seven cores are Berea sandstone (same wettability) and the fluids used and the injection rates are same, it is concluded that the difference of the exponent (a) is related to the pore structure of the cores. The results did not show a direct relationship between the exponent (a) and permeability of the core.

6 Comparing Models and Discussion

The present model has been compared with three models of relative permeability. This section presents the models, results of comparison and discussion.

Corey proposed a simple mathematical expression for generating the relative permeability data of the gas-oil system (Corey 1954; Ahmed 2001a). For drainage process, the relative permeability ratio from Corey's model (after changing oil by water) is:

$$\frac{K_{rg}}{K_{rw}} = \frac{(S_g^*)^3 (2 - S_g^*)}{(1 - S_g^*)^4} \quad (30)$$

where

$$S_g^* = \frac{S_g}{1 - S_{wc}} ,$$

and S_g is gas saturation.

Pirson derived from petrophysical considerations generalized relationships for determining the wetting and nonwetting phase relative permeability (Pirson 1958; Ahmed 2001a). For drainage process, the relative permeability ratio from Pirson's model is:

$$\frac{K_{rg}}{K_{rw}} = \frac{(1 - S_w^*)[1 - (S_w^*)^{0.25} (S_w)^{0.5}]^{0.5}}{(S_w^*)^{0.5} (S_w)^3} \quad (31)$$

where

$$S_w^* = \frac{S_w - S_{wc}}{1 - S_{wc}}$$

Kam and Rossen estimated relative-permeability functions for gas and liquid phases by curve-fitting data for unconsolidated sand packs (Collins 1961; Kam and Rossen 2003; Li 2006; Dholkawala et al. 2007):

$$K_{rg} = \left(\frac{1 - S_w - S_{gc}}{1 - S_{wc} - S_{gc}} \right)^{2.2868} \quad (32)$$

$$K_{rw} = 0.7888 \left(\frac{S_w - S_{wc}}{1 - S_{wc} - S_{gc}} \right)^{1.9575} \quad (33)$$

Thus the relative permeability ratio is:

$$\frac{K_{rg}}{K_{rw}} = \frac{\left(\frac{1 - S_w - S_{gc}}{1 - S_{wc} - S_{gc}} \right)^{2.2868}}{0.7888 \left(\frac{S_w - S_{wc}}{1 - S_{wc} - S_{gc}} \right)^{1.9575}} \quad (34)$$

It is noted that the exponents of relative permeability of gas and water of Kam and Rossen model have approximately the same value (2) which is similar to the exponent in Eqs. 15, and 16. The difference between the two models is that Kam and Rossen model includes fixed values for K_{rgwc} and K_{rwgc} with (1) and (0.7888), respectively, while in Eqs. 15, and 16, K_{rgwc} and K_{rwgc} should be determined experimentally.

It is necessary to remind that validity of the improved present model (representing by Eqs. 20, 28, and 29) is restricted by validity of the fractional flow equation (Eq. 19) at conditions of the displacement experiment. Eq. 19 assumes an incompressible steady-state flow in one dimension and negligible effects of the capillary pressure gradient and gravity (Dake 1978; Ahmed 2001b). In horizontal flow experiments the gravity effect can be neglected and using high injection rate reduces the capillary effect. In experiments of displacing liquid by gas with downward vertical flow (as in our experiments) the gravity effect is opposite to the capillary effect. This leads to cancel or at less to reduce both of them. Using the material balance equation to calculate the average water saturation overcomes the drawback of compressibility. Accuracy of approaching the unsteady-state by steady-state flow depends on the pressure gradient of flow. The unsteady-state flow with less pressure gradient is the closest to the steady-state flow.

Figs. 10 to 16 show comparisons between models of relative permeability in terms of gas/water relative-permeability ratio and fractional flow as a function of water saturation of seven cores. It is observed that the gas/water relative-permeability ratio of present model is close to Pirson, and Kam and Rossen models at the range of ($0.7 < S_w < 0.9$) almost in all cores. Corey model gives higher relative-permeability ratio than other models for all cores at water saturations below (0.8). Pirson model gives higher relative-permeability ratio at water saturations above (0.9). Fractional flow curves of core A in Fig. 10 shows that the straight line between the initial conditions (point with co-ordinates $S_w = 1$, $f_w = 1$) and the conditions at the gas breakthrough determined experimentally (point with co-ordinates $S_w = (S_{wavg})_{Bth}$, $f_w = 0$) is a tangent only for curves of the present and Corey models. Fractional flow curves of core B in Fig. 11 shows that the straight line is a tangent only for curves of the present, and Kam and Rossen models. For the other cores the straight line is a tangent only for curve of the present model. Thus the straight line is a tangent of curve of the present model for all cores. This is because the present model is included adjustment of the exponent (a) to match the displacement performance.

In Figs. 10, and 11 the tangency points of the present model are different from that of Corey, and Kam and Rossen models, respectively. This means different results of saturation and fractional flow at the displacement front, but the average saturation for core A is same from the present and Corey models, and for core B is same from the present, and Kam and Rossen models. To clarify this point, we will use core A. The saturation profile at any dimensionless time expressed by the injected pore volume can be constructed from Buckley-Leverett (1942) Eq.:

$$\frac{X}{L} = PV\left(\frac{df_w}{dS_w}\right)_{S_w} \tag{35}$$

where X = the position of S_w, L = the length of core sample (X and L should be with same units), PV = the injected pore volume (dimensionless), and (df_w/dS_w) = the derivative of fractional flow with respect to water saturation (dimensionless). (df_w/dS_w) of the present model can be obtained from differentiating Eq. 21 with respect to water saturation:

$$\left(\frac{df_w}{dS_w}\right) = \frac{\dfrac{a(1-S_{wc}-S_{gc})\mu_w K_{rgwc}}{(S_w-S_{wc})(1-S_w-S_{gc})\mu_g K_{rwgc}}\left(\dfrac{1-S_w-S_{gc}}{S_w-S_{wc}}\right)^a}{\left[1+\dfrac{\mu_w K_{rgwc}}{\mu_g K_{rwgc}}\left(\dfrac{1-S_w-S_{gc}}{S_w-S_{wc}}\right)^a\right]^2} \tag{36}$$

(df_w/dS_w) of Corey model can be obtained from Substituting Eq. 30 in Eq. 19 then differentiating with respect to water saturation:

$$\left(\frac{df_w}{dS_w}\right) = \frac{-\dfrac{2\mu_w(1-S_w)^2\left[(S_w-S_{wc})(3S_{wc}-2S_w-1)-2(1-S_w)(1+S_w-2S_{wc})\right]}{\mu_g(S_w-S_{wc})^5}}{\left[1+\dfrac{\mu_w(1+S_w-2S_{wc})(1-S_w)^3}{\mu_g(S_w-S_{wc})^4}\right]^2} \tag{37}$$

Fig. 17 shows a comparison between the present and Corey models in terms of water saturation profile calculated by Eq. 35 at the gas breakthrough of core A. Although the saturation profiles are not identical but the areas above the profiles which represent the water-recovery fraction are equal. The areas below the two saturation profiles are represent the average water saturation and they are also equal for the two models. This can be proved mathematically. From Eq. 35, at the breakthrough moment (X/L) = 1, and curves of the present and Corey models in Fig. 10b have the same tangent i.e. same (df_w/dS_w), in spite of the different tangency points, thus to satisfy Eq. 35, it should be the same injected pore volume for the two models. The real injected pore volume at the breakthrough moment equals the water-recovery fraction and it is same the average gas saturation in the core. Saturation profile of Corey model in Fig. 17 shows that the gas saturation is almost constant along the core, while the present model shows there is a gradient in gas saturation which is the closest to the actual displacement process.

It is concluded that the present model can match the displacement performance by considering fluids rheology and parameters characterizing behavior of the porous medium during the displacement process. This is an important advantage to improve modeling of displacement experiments, and to improve understanding of mechanisms of enhanced oil recovery techniques such as injection of different chemicals alternately, water-alternating-gas injection, and foam flooding.

7 Conclusions

1. Two functions of porosity and permeability were derived from capillary-bundle model. The functions represent number of capillaries and the average diameter of capillaries.
2. A generalized function called poroperm function was derived from the number of capillaries. The poroperm can be used to evaluate the dynamic pore connectivity of porous media.
3. A preliminary model of relative permeability was derived from the poroperm function. The model is based on an assumption is existed implicitly in the modified Brooks and Corey model.
4. The preliminary model was improved to match displacement experiments whenever the fractional flow theory is applicable.
5. Advantage of the improved model over previous models is to consider fluids viscosities, and the average saturation the moment of the breakthrough in addition to other parameters considered by previous models.

References

Ahmed, T. (2001a). Reservoir Engineering Handbook. (2nd ed). USA: Butterworth-Heinemann, (Chapter 5).

Ahmed, T. (2001b). Reservoir Engineering Handbook. (2nd ed). USA: Butterworth-Heinemann, (Chapter 14).

Alpak, F.O., Lake, L. W., and Embid, S.M. (1999). Validation of a Modified Carman-Kozeny Equation To Model Two-Phase Relative Permeabilities. Proceedings of Annual Technical Conference and Exhibition of Society of Petroleum Engineers, 3-6 October, Houston, Texas, USA, SPE 56479.

Bang, V., Kumar, V., Ayyalasomayajula, P.S., Pope, G.A. and Sharma, M.M. (2006). Relative Permeability of Gas-Condensate Fluids: A General Correlation. Proceedings of Annual Technical Conference and Exhibition of Society of Petroleum Engineers, 24-27 September, San Antonio, Texas, USA, SPE 102741.

Bech, N., Olsen, D., and Nielsen, C.M. (2000). Determination of Oil/Water Saturation Functions of Chalk Core Plugs From Two-Phase Flow Experiments. Journal of SPE Reservoir Evaluation & Engineering, **3**(1), 50-59.

Behrenbruch, P., and Goda, H.M. (2006). Two-Phase Relative Permeability Prediction: A Comparison of the Modified Brooks-Corey Methodology with a New Carman-Kozeny Based Flow Formulation. Proceedings of Asia Pacific Oil & Gas Conference and Exhibition of Society of Petroleum Engineers, 11-13 September, Adelaide, Australia, SPE 101150.

Buckley, S.E. and Leverett, M.C. (1942). Mechanism of fluid displacement in sands. Petroleum Transactions, AIME, **146**, 107-116.

Collins, R.E. (1961). Flow of Fluids Through Porous Materials. Englewood, Colorado, USA: Research & Engineering Consultants, Inc.

Corey, A.T. (1954). The interrelation between gas and oil relative permeabilities. Producers Monthly, **19**(1), 38-41.

Dake, L.P. (1978). Fundamentals of Reservoir Engineering. Amsterdam, The Netherlands: Elsevier Science B.V., (Chapter 10).

Dholkawala, Z.F., Sarma, H.K., and Kam, S.I. (2007). Application of Fractional Flow Theory to Foams in Porous Media. Journal of Petroleum Science & Engineering, Elsevier, 57,152-165.

Fanchi, J.R. (2001). Principles of Applied Reservoir Simulation. (2nd ed). USA: Gulf Professional Publishing. Elsevier, (Chapter 14).

Honarpour, M., Koederitz, L.F., and Harvey, A. H. (1986). Relative Permeability of Petroleum Reservoir. Florida, Boca Raton, USA: CRC Press, Inc.

Honarpour, M., Koederitz, L.F., and Harvey, A.H. (1982). Empirical Equations of Estimating Two-Phase Relative Permeability in Consolidated Rock. Journal of Petroleum Technology, **34**(12), 2905-2908

Ibrahim, M.N.M., and Koederitz, L.F. (2000). Two-Phase Relative Permeability Prediction Using a Linear Regression Model. Proceedings of Eastern Regional Meeting of Society of Petroleum Engineers, 17-19 October , Morgantown, West Virginia, USA, SPE 65631.

Ibrahim, M.N.M., and Koederitz, L.F. (2001). Two-Phase Steady-State and Unsteady-State Relative Permeability Prediction Models. Proceedings of Middle East Oil Show of Society of Petroleum Engineers, 17-20 March, Bahrain, SPE 68065.

Jones, S.C., Roszelle, W.0. (1978). Graphical Techniques for Determining Relative Permeability From Displacement Experiments. Journal of Petroleum Technology. **30**(5), 2905-2908.

Kam, S.I., and Rossen, W.R. (2003). A Model for Foam Generation in Homogeneous Media. Journal of Society of Petroleum Engineers, **8**(4), 417-425.

Li, K. (2008). A New Method for Calculating Two-Phase Relative Permeability from Resistivity Data in Porous Media. Transport in Porous Media, **74**, 21–33.

Li, K., Shapiro, M., Horne, R.N., Ma, S., Hajari, A., Mudhhi, M. (2010). In Situ Estimation of Relative Permeability from Resistivity Measurements. Proceedings of the International Oil and Gas Conference and Exhibition of Society of Petroleum Engineers in China, 8-10 June 2010, Beijing, China, SPE 129627.

Li, Q. (2006). Foam Generation and Propagation in Homogeneous and Heterogeneous Porous Media. Ph.D. Dissertation, The University of Texas at Austin, p.202.

Mitlin, V.S., Lawton, B. D., McLennan, J.D., and Owen, L.B. (1998). Improved Estimation of Relative Permeability from Displacement Experiments. Proceedings of the International Petroleum Conference and Exhibition of Mexico, 3-5 March, Villahermosa, Mexico, SPE 39830.

Pirson, S. J. (1958). "Petrophysics", Oil Reservoir Engineering. (2nd ed). New York, USA: McGraw-Hill Book Co., Inc.

Silpngarmlers, N., Guler, B., Ertekin, T., and Grader, A.S. (2002). Development and Testing of Two-Phase Relative Permeability Predictors Using Artificial Neural Networks. Journal of Society of Petroleum Engineers, **7**(3), 299-308.

Tiab, D., and Donaldson, E.C. (2004). Petrophysics: Theory and Practice of Measuring Reservoir Rock and Fluid Transport Properties. (2nd ed). USA: Elsevier, Inc., (Chapter 7) p.425.

Torcaso, M. A., and Wyllie, M. R. J. (1958). A Comparison of Calculated k_{rg}/k_{ro} Ratios with Field Data. Journal of Petroleum Technology. **10**(12), 57-58

Torsæter, O., and Abtahi, M. (2003). Experimental Reservoir Engineering, Laboratory Workbook. Dept. of Petroleum Eng. and Applied Geophysics, Norwegian University of Science and Technology , (Chapter 11).

Toth, J., Bodi, T., Szucs, P. and Civan F. (2001). Direct Determination of Relative Permeability from Nonsteady-State Constant Pressure and Rate Displacements. Proceedings of Production and Operations Symposium of Society of Petroleum Engineers, 24-27 March, Oklahoma City, Oklahoma, USA, SPE 67318.

Toth, J., Bodi, T., Szucs, P. and Civan F. (1998). Practical Method for Analysis of Immiscible Displacement in Laboratory Core Tests. Transport in Porous Media **31,** 347–363.

Welge, H.J. (1952). A Simplified Method for Computing Oil Recovery by Gas or Water Drive. Petroleum Transactions, AIME, **195**, 91-98.

Wyllie, M.R.J., and Gardner, G.H.F. (1958). The Generalized Kozeny-Carmen Equation-Its Application to Problems of Multi-Phase Flow in Porous Media. World Oil, **146**, 121.

Table 1 Properties of brine and nitrogen gas at room conditions (0.994 atm and 25 ºC)

Materials	**Viscosity (mPa.sec)**		**Density (g/cc)**	
	Determination Method	**Result**	**Determination Method**	**Result**
Brine	Measured by Capillary Viscometer	1.1361	Measured by Density Meter	1.0155
Nitrogen Gas	Calculated from Correlation of Manual of Bench Top Permeability System	0.0176432	Calculated from Gases Law	0.001145

Table 2 Properties of cores and results of gas relative permeability at the irreducible water saturation

Core Id.	**Diam., cm**	**Length, cm**	**Porosity %**	***K*, μm^2**	S_{wc}	K_{rgwc}
A	3.832	3.925	13.487	1.93×10^{-3}	0.619	0.430
B	3.795	3.894	16.710	32.96×10^{-3}	0.558	0.266
C	3.795	3.895	17.818	9.71×10^{-3}	0.522	0.483
D	3.815	5.452	12.226	5.30×10^{-4}	0.442	0.761
E	3.808	2.592	20.559	22.96×10^{-3}	0.588	0.312
F	3.799	7.718	16.599	67.11×10^{-3}	0.483	0.276
G	3.794	7.627	18.023	109.04×10^{-3}	0.665	0.188

Table 3 The average water saturation behind the front at the breakthrough moment, exponent (a), and water saturation and fractional flow at the front

Core Id.	$(S_{wavg})_{Bth}$	**Exponent (a)**	S_{wf}	f_{wf}
A	0.892	1.849	0.942	0.463
B	0.893	1.456	0.960	0.626
C	0.797	3.101	0.840	0.213
D	0.803	2.738	0.856	0.269
E	0.852	2.014	0.910	0.393
F	0.862	1.546	0.942	0.579
G	0.852	2.063	0.902	0.338

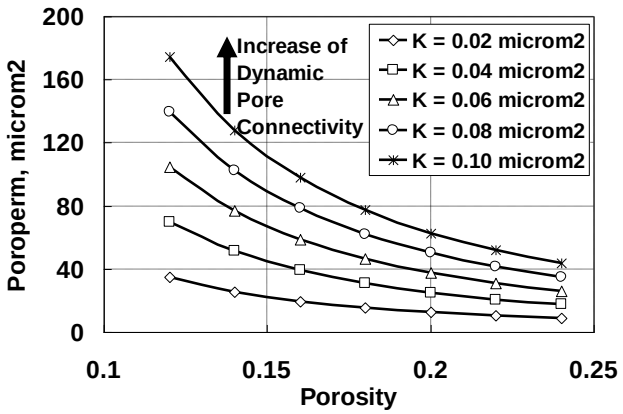

Fig. 1 Relationship of the poroperm function with the porosity at different permeabilities

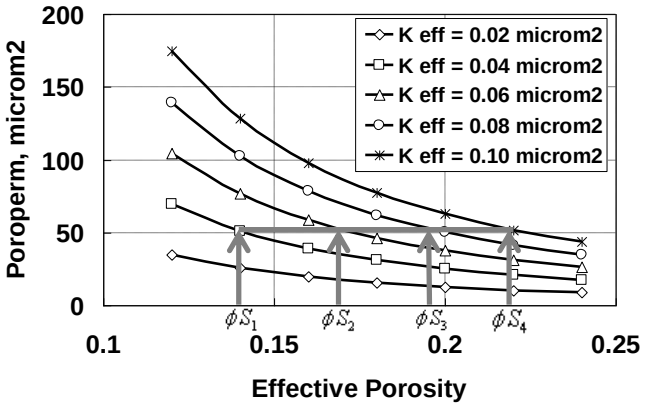

Fig. 2 Change of the effective permeability with effective porosity at the same poroperm

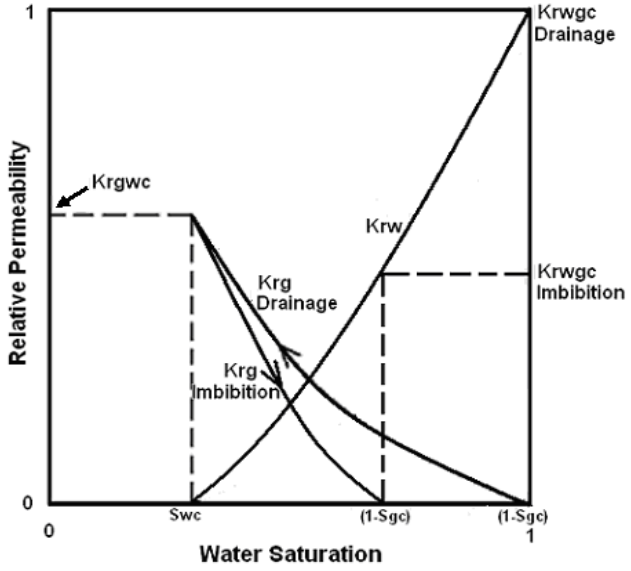

Fig. 3 Typical relative permeability relationship of water-gas system in a core was initially saturated with water.

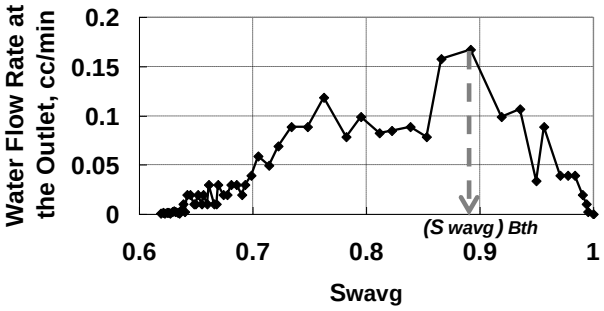

Fig. 4 Determination of $(S_{wavg})_{Bth}$ from water flow rate at the core outlet (data of core A)

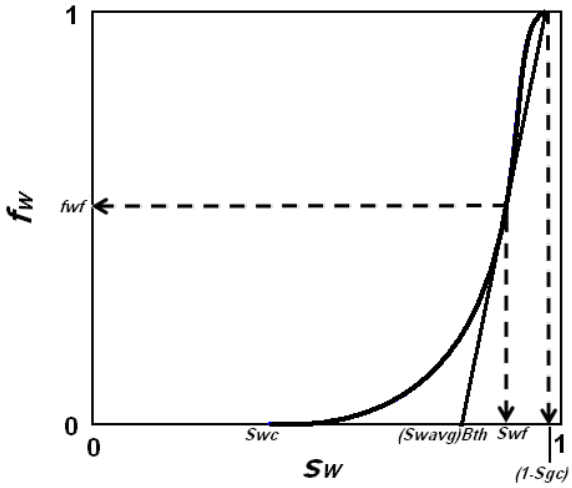

Fig. 5 Welge's technique to determine the average water saturation behind the front at moment of gas breakthrough ($(S_{wavg})_{Bth}$).

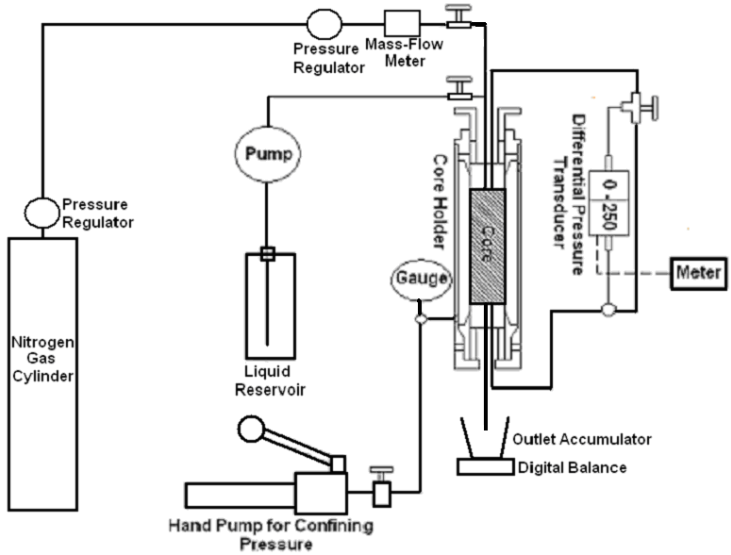

Fig. 6 Diagram of Bench Top Permeability System

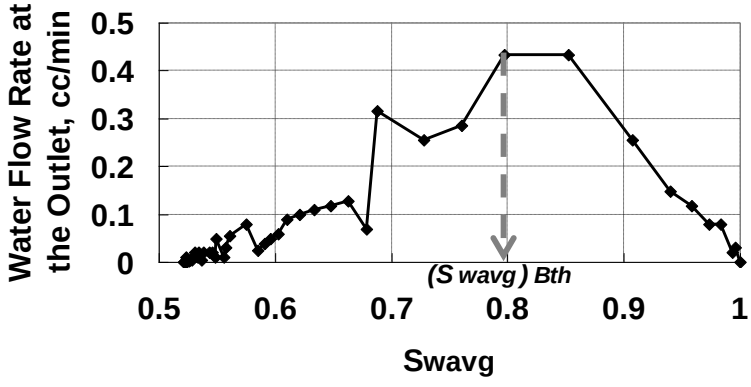

Fig. 7 Determination of $(S_{wavg})_{Bth}$ from water flow rate at the outlet of core C. The flow rate stabilized before the gas breakthrough.

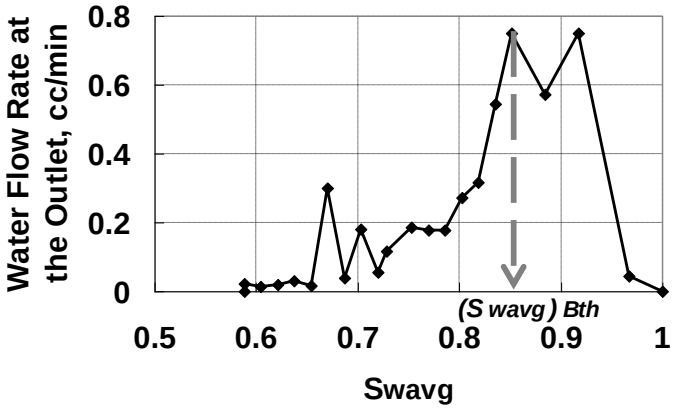

Fig. 8 Determination of $(S_{wavg})_{Bth}$ from water flow rate at the outlet of core E. The water flow rate oscillates before the actual breakthrough of the continuous gas stream because of the gas compressibility or slipping of some of separate bubbles of gas ahead of the continuous gas stream.

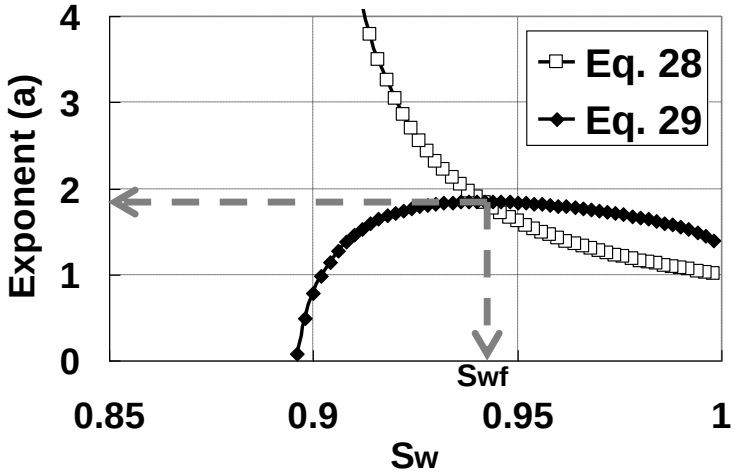

Fig. 9 Determination of the exponent (a) and S_{wf} for displacement process of core A.

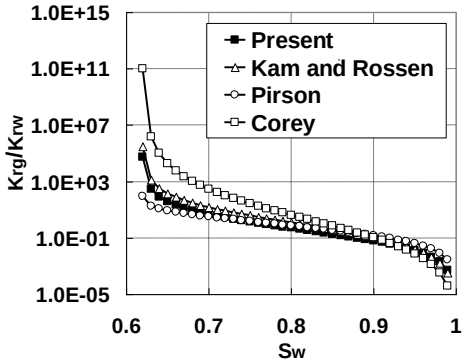

(a)

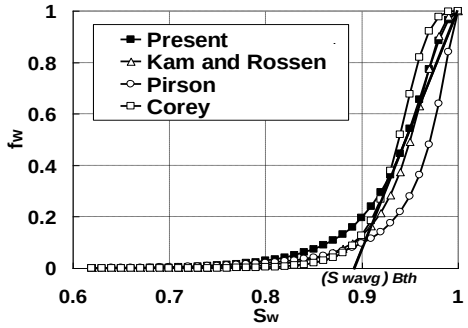

(b)

Fig. 10 Comparison between models of relative permeability for core A: (a) Relative permeability ratio. (b) Fractional flow curve.

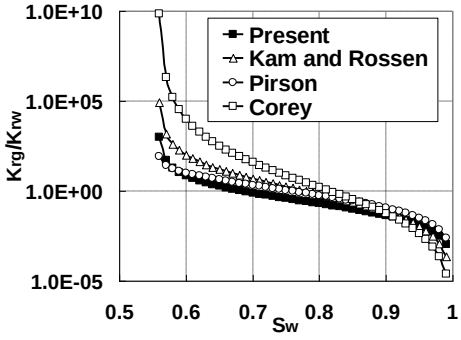

(a)

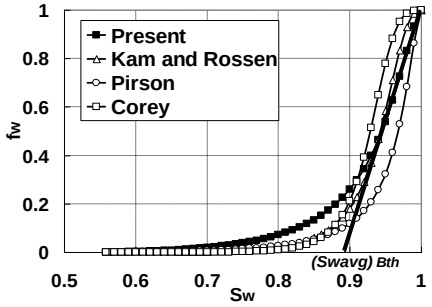

(b)

Fig. 11 Comparison between models of relative permeability for core B: (a) Relative permeability ratio. (b) Fractional flow curve.

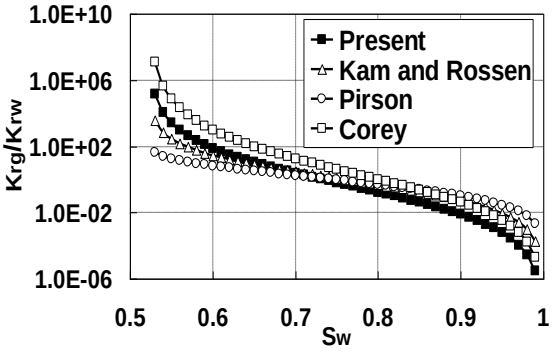

(a)

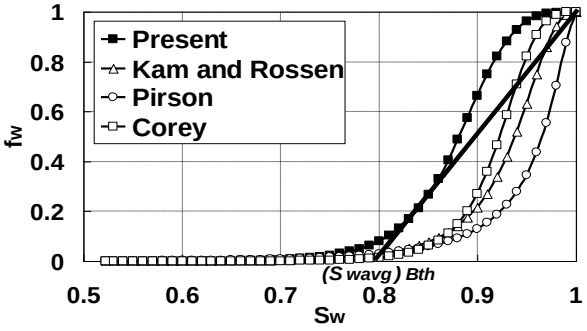

(b)

Fig. 12 Comparison between models of relative permeability for core C: (a) Relative permeability ratio. (b) Fractional flow curve.

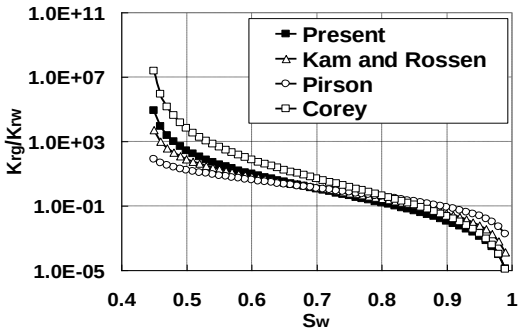

(a)

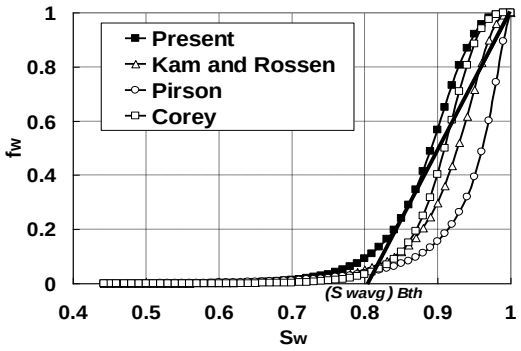

(b)

Fig. 13 Comparison between models of relative permeability for core D: (a) Relative permeability ratio. (b) Fractional flow curve.

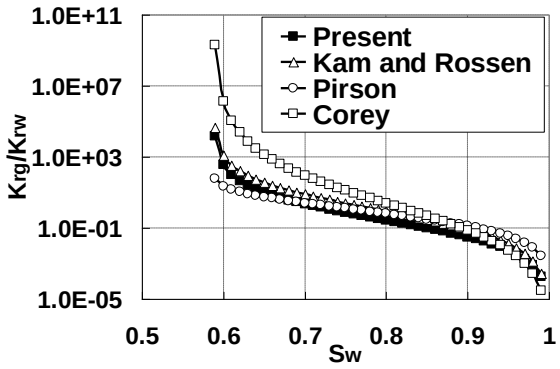

(a)

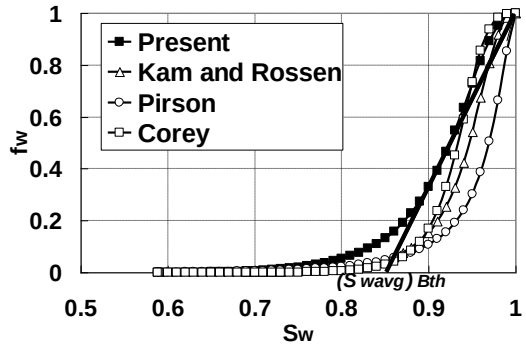

(b)

Fig. 14 Comparison between models of relative permeability for core E: (a) Relative permeability ratio. (b) Fractional flow curve.

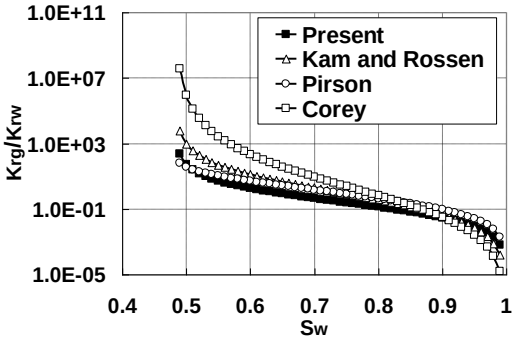

(a)

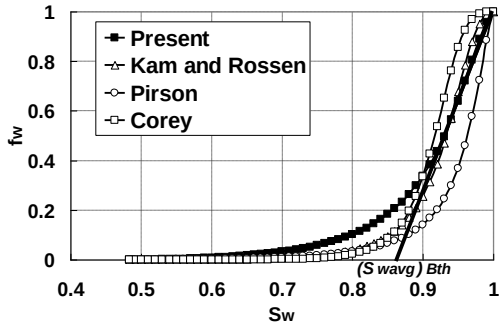

(b)

Fig. 15 Comparison between models of relative permeability for core F: (a) Relative permeability ratio. (b) Fractional flow curve.

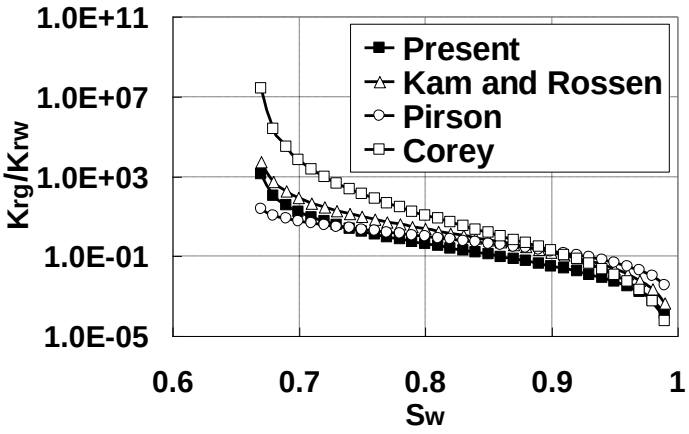

(a)

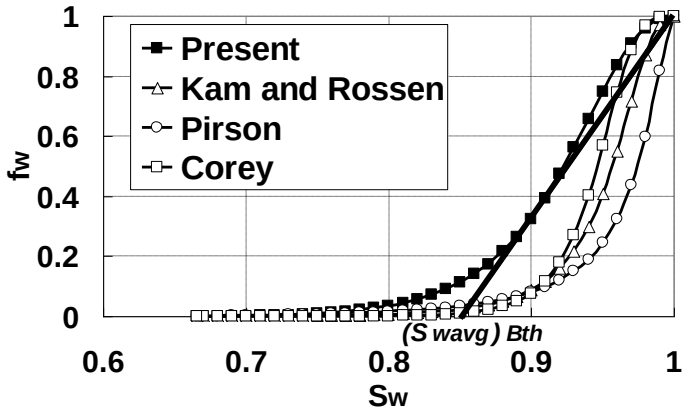

(b)

Fig. 16 Comparison between models of relative permeability for core G: (a) Relative permeability ratio. (b) Fractional flow curve.

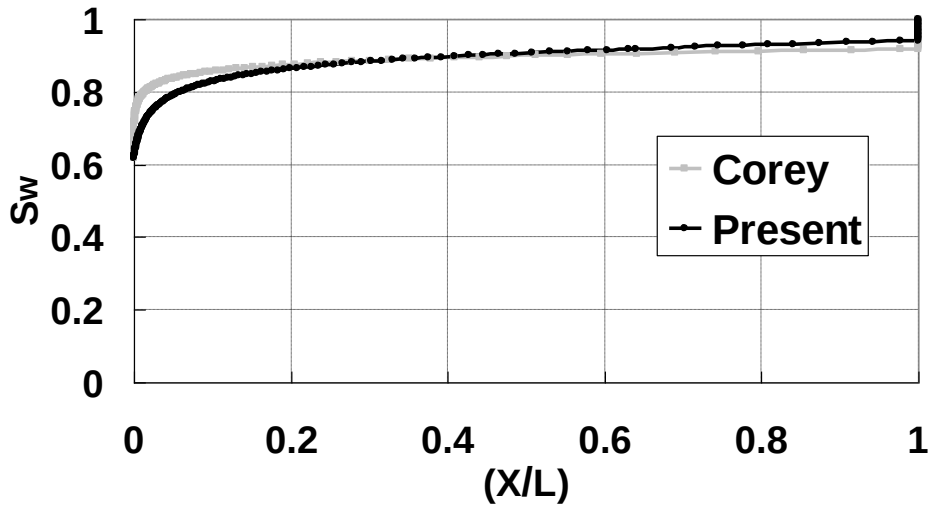

Fig. 17 Comparison between the present and Corey models in terms of water saturation profile at the gas breakthrough of core A.